Oxidation State, Coordination, and Covalency Controls on Iron Isotopic Fractionation in Earth's Mantle and Crust

Marc Blanchard, Nicolas Dauphas

14

Oxidation State, Coordination, and Covalency Controls on Iron Isotopic Fractionation in Earth's Mantle and Crust: Insights from First-Principles Calculations and NRIXS Spectroscopy

Marc Blanchard[1] and Nicolas Dauphas[2]

ABSTRACT

Isotopes provide valuable insights into the complex geochemical behavior of iron. To put the wealth of Fe isotopic data measured in natural samples into a quantitative framework, it is important to know how iron isotopes are fractionated at equilibrium between co-existing iron-bearing phases or species. These isotopic equilibrium fractionation factors can be derived from isotopic exchange experiments and the study of natural samples, but can also be calculated from partition functions, whose main contribution is the vibrational energy. This approach relies on first-principles calculations (atomistic modeling based on quantum mechanics) and vibrational spectroscopies (Mössbauer and Nuclear Resonant Inelastic X-ray Scattering – NRIXS). Comparison of the results obtained from these techniques provides confidence in their reliability and improves our understanding of the parameters controlling iron isotopic fractionation among coexisting phases. After an introduction to the theory and methods applied in this field, the chapter will review how NRIXS and first-principles calculations help interpret iron isotopic variations in natural rocks and minerals. At equilibrium, the heavy isotopes of iron will concentrate in the phases where the interatomic force constants are the greatest, meaning in the phases where iron bonds are the stiffest. Higher oxidation state, higher covalency, and lower coordination (shorter bond length) tend to be associated with stronger bonds and heavy iron isotope enrichments.

14.1. INTRODUCTION

Iron is a ubiquitous element that is abundant in terrestrial rocks, fluids, and magmas. It displays a rich and complex chemistry based on its multiple valence. Its three oxidation states are 0 (metallic iron), +2 (ferrous iron), and +3 (ferric iron). On Earth, these oxidation states are stratified in a manner that follows the structural and chemical layers characterizing our planet. At the center, the core is made of metallic iron alloyed with some lighter elements. The mantle is the main repository for ferrous iron under the form of silicate and oxide minerals. Ferric iron is mainly found in crustal rocks and surface environments due to the presence nowadays of an oxygen-rich atmosphere.

Iron chemical behavior is often involved in oxidation-reduction (redox) equilibria: chemical reactions that involve a transfer of electrons between species having different valence states. This electron transfer implies a

[1]*Géosciences Environnement Toulouse, Centre National de la Recherche Scientifique, Toulouse, France*

[2]*Department of the Geophysical Sciences, The University of Chicago, Chicago, USA*

Magma Redox Geochemistry, Geophysical Monograph 266, First Edition.
Edited by Roberto Moretti and Daniel R. Neuville.

DOI: 10.1002/9781119473206.ch14

readjustment of chemical bonds. As we will see, the modification of the interatomic bonds affects in turn the isotopic properties. The ubiquity and rich chemistry of iron explains why variations in its four stable isotopes (^{54}Fe, ^{56}Fe, ^{57}Fe, and ^{58}Fe) have become essential tools to investigate various cosmochemical, geochemical, and biochemical questions. In Earth sciences, iron isotopic analyses have brought new insights into planetary accretion and mantle-core differentiation, crust formation by partial melting, redox evolution of the Earth's mantle, redox evolution of the ocean in relation with the oxygenation of the atmosphere, and magmatic differentiation. An overview of the most recent results on these topics can be found in Dauphas and Rouxel (2006), Johnson et al. (2008), and Dauphas et al. (2017).

The relative enrichment in heavy isotopes of one phase relative to another referred to as isotope fractionation, can be due to kinetic processes or can occur in conditions of thermodynamic equilibrium. Equilibrium isotopic fractionation factors represent reference values that must be known in order to interpret the iron isotope variations measured on natural samples. These key data and their temperature dependence can be obtained through several approaches. The most traditional way consists in designing isotope exchange experiments whose goal is to attain or to point to the equilibrium state (e.g., Schuessler et al., 2007; Shahar et al., 2008, 2017; Saunier et al., 2011; Syverson et al., 2013). Alternative approaches consist of deriving theoretically the equilibrium isotopic fractionation factors from the measurement or the computation of vibrational properties. Electronic structure calculations based on the resolution of quantum mechanics' laws can be used for determining the equilibrium fractionation for any traditional or non-traditional stable isotopes (e.g., Schauble, 2004; Blanchard et al., 2017). This theoretical approach is also of great interest for investigating what crystal chemical parameters govern the isotopic fractionation. Alternatively, for Mössbauer-active elements (like iron), the vibrational properties of the target element in solids can be investigated by Mössbauer spectroscopy through the measurement of the temperature dependence of the isomer shift (e.g., Polyakov & Mineev, 2000) or using nuclear resonance inelastic X-ray scattering, NRIXS (e.g., Polyakov et al., 2005; Dauphas et al., 2012, 2018). While sound theoretically, determining the second-order Doppler shift via the temperature dependence of the isomer shift in Mössbauer spectroscopy is fraught with difficulties. The NRIXS technique provides the vibrational density of states for the resonant atom and the database of equilibrium fractionation factors calculated from NRIXS measurements is rapidly growing.

In this chapter, we will give a brief introduction to the theory of mass-dependent stable isotope fractionation. We will define the quantity that is actually calculated (i.e., the reduced partition function ratio β) and how it relates with the commonly used fractionation factor α. We will explain how the β-factor is derived from atomistic modeling or NRIXS measurements. Iron isotope studies based on these two techniques will be reviewed, focusing on minerals and melts. The reliability of the derived equilibrium fractionation factors will be assessed by comparing the results from the various techniques. The results will be analyzed to identify what are the crystal parameters that control the equilibrium fractionation factors. The final section of this chapter will discuss some examples of igneous systems where equilibrium fractionation factors help assess how iron geochemistry and redox behavior affect iron isotopic variations.

14.2. THEORY: EQUILIBRIUM ISOTOPIC FRACTIONATION FROM VIBRATIONAL PROPERTIES

The theory of equilibrium mass-dependent stable isotope fractionation has been established by Bigeleisen and Mayer (1947) and Urey (1947). Here we define briefly the fractionation factors α and β, and we introduce the expressions that are used for determining their theoretical values. More details can be found in the review article of Blanchard et al. (2017).

Let's consider a reaction during which the X' (light) and X (heavy) isotopes are exchanged between two phases A and B:

$$AX' + BX \rightleftarrows AX + BX' \tag{14.1}$$

Even in conditions of thermodynamics equilibrium, the isotopic exchange leads to an isotopic enrichment of one phase relative to the other. This phenomenon of equilibrium isotopic fractionation has some temperature dependence that can be calculated. Indeed, as any chemical reaction, the isotopic exchange reaction is characterized by an equilibrium constant, K_{eq}, related to the variation of the standard free energy between reactants and products, or to the partition functions, Q, of the reactants and products; the two quantities (free energy and partition function) being linked. The equilibrium constant of Reaction 14.1 is thus given by the following expression:

$$K_{eq} = \frac{Q_{products}}{Q_{reactants}} = \frac{Q(AX) \times Q(BX')}{Q(AX') \times Q(BX)} \tag{14.2}$$

The commonly used fractionation factor, α, between two phases can be defined as the ratio of quantum and classical equilibrium constants (i.e., equilibrium constants obtained considering either quantum or classical mechanics). This is justified by the fact that classical contributions to the partition functions only play a bookkeeping role in

the isotopic fractionation, and therefore it is convenient to define a reduced partition function, by ratioing the quantum partition function to its classical counterpart (Q_{qm}/Q_{cl}). Thus using Equation 14.2, the α fractionation factor between phases AX and BX can be expressed as:

$$\alpha_{AX-BX} = \frac{(K_{eq})_{qm}}{(K_{eq})_{cl}} = \frac{Q_{qm}(AX) \times Q_{cl}(AX')}{Q_{qm}(AX') \times Q_{cl}(AX)} \times \frac{Q_{qm}(BX') \times Q_{cl}(BX)}{Q_{qm}(BX) \times Q_{cl}(BX')} = \frac{\beta_{AX}}{\beta_{BX}} \quad (14.3)$$

This expression allows introducing the concept of reduced partition function ratio, also called β. The reduced partition function ratio β_{AX} can be seen as the isotopic fractionation factor between the phase AX and an ideal atomic gas of X. Contrary to the fractionation factor α that can be measured directly from isotope exchange experiments where two or more phases are coexisting, the fractionation factor β is associated to one phase, and in most cases, cannot be retrieved from isotopic compositions. However, β is the quantity that is calculated from the vibrational properties, as described below. As shown in Figure 14.1, β-factors can be conveniently compared and combined in order to derive the equilibrium fractionation factors α between any coexisting phases. Isotopic fractionations are relatively small, on the order of parts per thousand for iron isotopes, so it is common to use the notation 1000 ln α or 1000 ln β, reporting the result in permil (‰).

From Equation 14.3, we understand that the β-factor of a given phase can be calculated from the classical and quantum partition functions. Their expressions are explained and detailed in several articles (e.g., Bigeleisen & Mayer, 1947; Richet et al., 1977). Briefly, the ratio of the classical partition functions of two isotopologues will only depend on the atomic mass of isotopes and symmetry considerations, while the main contribution to the quantum partition function is the vibrational energy. If we consider a crystal undergoing a complete isotopic substitution and if interatomic vibrations are treated as harmonic, we obtain the following β-factor expression:

$$\beta_{AX} = \left[\prod_{i=1}^{3N} \prod_{\{q\}} \frac{\nu_{q,i}}{\nu'_{q,i}} \times \frac{e^{-h\nu_{q,i}/(2kT)}}{1-e^{-h\nu_{q,i}/(kT)}} \times \frac{1-e^{-h\nu'_{q,i}/(kT)}}{e^{-h\nu'_{q,i}/(2kT)}} \right]^{1/nN_q} \quad (14.4)$$

where $\nu_{q,i}$ and $\nu'_{q,i}$ are the vibrational frequencies of the vibrational mode i = 1,3N along wavevector q for the two isotopologues. N is the number of atoms in the crystal unit-cell with n sites for the element of interest. T is the temperature, h the Planck constant and k the Boltzmann constant. The second product is performed on a sufficiently large grid of N_q q-points in the first Brillouin zone. Crystal lattices have some periodicity that can be captured by their Fourier transform, which is also a lattice known as reciprocal space. The first Brillouin zone is a primitive cell in the reciprocal space and this zone is sampled using a uniform grid of q-points. β-factor value converges toward the final value while the number of q-points used is increased. The expression 14.4 takes into account the "rule of the high-temperature product" also called "Redlich-Teller rule" (Kieffer, 1982), which accounts for the fact that there should be no isotopic fractionation in the high-temperature limit. Similar β-factor expressions can be derived for a molecule where rotational and translational motions also contribute to the partition function or for the case of a "site by site" isotopic substitution (Blanchard et al., 2017).

In an equivalent way, one can write the equilibrium fractionation factor β as a function of the kinetic energy K of the element (Polyakov, 1997):

$$ln\,\beta_{AX} = \frac{m-m'}{m}\left(\frac{K}{RT} - \frac{3}{2}\right) \quad (14.5)$$

Here this kinetic energy will be calculated from the vibrational density of states of the element $g(e)$:

$$K = \frac{3}{2}\int_0^{e_{max}} E(e/kT)g(e)de \quad (14.6)$$

where $E(e/kT)$ is the Einstein function for the vibrational energy of a single harmonic oscillator at frequency $\nu = e/h$, and e_{max} corresponds to the maximal energy of the vibrational spectrum. Using a series expansion of the kinetic energy above (Polyakov et al., 2005, 2007) or a Bernoulli

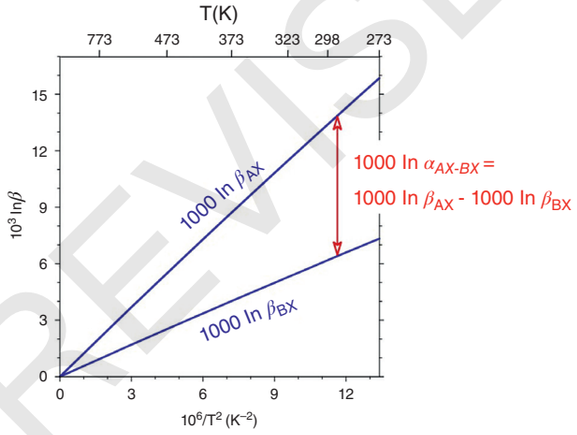

Figure 14.1 Generic example of the temperature dependence of the β-factors of phases AX and BX, expressed in ‰. β-factors can then be combined in order to obtain the equilibrium fractionation factor α between these two phases; a quantity that can be compared to measured isotopic fractionations between co-existing phases.

expansion of the β-factor (Dauphas et al., 2012), the β-factor can be expressed as,

$$ln\,\beta_{AX} = \left(\frac{m'}{m} - 1\right)\left(\frac{m_2^g}{8k^2T^2} - \frac{m_4^g}{480k^4T^4} + \frac{m_6^g}{20160k^6T^6}\right) \quad (14.7)$$

where m_i^g is the ith moment of the vibrational density of states $g(e)$: $m_i^g = \int_0^+ {}^{\infty} g(e)e^i de$

Finally, Bigeleisen and Mayer (1947) also derived an approximate formula, which relates the β-factor to the force constants (the equivalent of a spring constant for a mechanical spring) acting on the element of interest:

$$\beta_{AX} = 1 + \frac{m - m'}{mm'}\frac{\hbar^2 F}{8(kT)^2} \quad (14.8)$$

with $\hbar = h/2\pi$. The mean force constant F is related to the second moment of the phonon density of states through Lipkin's sum rule (Lipkin, 1995, 1999), such that Equation 14.8 is equivalent to truncating Equation 14.7 to the first order (Dauphas et al., 2012). F is the sum of force constants in three orthogonal directions opposing displacement of the atom X from its equilibrium position. This expression is a valid approximation of Equation 14.4 when $h\nu/kT < 2$; in other words at high-temperature or for a system with relatively low relevant vibrations. For iron, Equation 14.7 is well approximated by Dauphas et al. (2012, 2017),

$$ln\,\beta_{AX} \approx 2.9\frac{F}{T^2} - 38\frac{F^2}{T^4} \quad (14.9)$$

Accordingly, truncating the expansion to the first term in the expansion, which is known as the high temperature approximation, gives rise to a relative error on $ln\beta_{AX}$ of $\sim 13F/T^2$, meaning that it will be larger for solids that have iron in stiff bonds and it will be smaller at high temperature (see Figure 14.2; Dauphas et al., 2012).

In conclusion of this theoretical section, one has to remember that the equilibrium fractionation factor α can be predicted by combining the relevant β-factors, which in turn are obtained from the vibrational properties. In practice, the variation of vibrational frequencies associated with the isotopic substitution, the vibrational density of states or the force constants of the element of interest can be determined either from first-principles calculations or by NRIXS spectroscopy, as we will see in the next section. Alternatively, although less accurate, it is possible to estimate the force constants using an ionic model based on Pauling's rules, mainly from the valences and ionic radii of the targeted element and its first neighbors. A derivation of this approach and an application to iron isotopes can be found in Young et al. (2015), Macris et al. (2015), and in Sossi and O'Neill (2017).

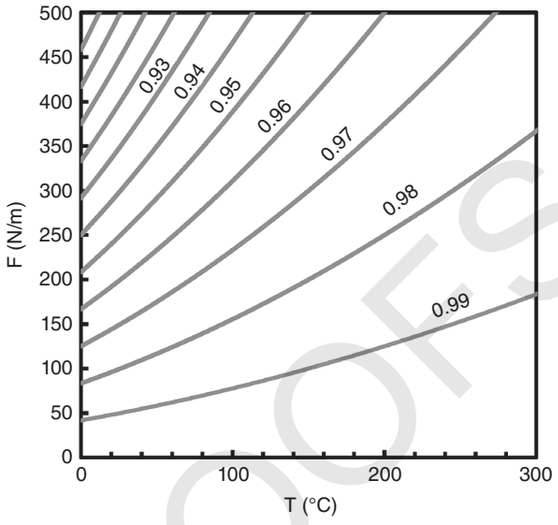

Figure 14.2 Relative departure (numbers on the curves) from Equation 14.8 introduced by the addition of the higher order term, for the $^{56}Fe/^{54}Fe$ ratio. For high-temperatures and relatively low force constants, equation (22.8) is a good approximation (Source: Dauphas et al., 2012. Reproduced with permission of Elsevier).

14.3. CALCULATION OF VIBRATIONAL PROPERTIES

14.3.1. First-Principles Calculations

The vibrational properties (vibrational frequencies, vibrational densities of states) can be calculated from atomistic modeling, which describes the behavior of a physicochemical system from its components at the atomic level. One can consider the ions and treat their interactions using classical mechanics using empirical force fields but most studies investigating non-traditional stable isotopes, and in particular iron isotopes, employ first-principles calculations. This means that the laws of quantum mechanics are used for describing the interactions between nuclei and electrons. In that case, the electronic structure is obtained by solving the Schrödinger equation requiring some approximations but no empirical parameters. A widespread class of first-principles calculations is based on the density functional theory (DFT), which considers that the ground state energy is a functional of the electronic density (Hohenberg & Kohn, 1964). More details about the computational techniques can be found in many books like for instance in the review by Cygan and Kubicki (2001).

There are typically three steps in first-principles calculations for obtaining the vibrational properties needed for the determination of equilibrium isotope fractionation

factors using either Equation 14.4, 14.5, or 14.8. In the first step, the minimum-energy structure is determined via geometric relaxation. From an initial guess geometry, often the experimentally determined structure, the forces on each atom, and the stress over the cell are calculated, and a refined guess structure is determined. This procedure continues iteratively until the residual forces and stress are sufficiently small. This relaxation is needed as otherwise the structure is unstable and calculation of vibrational frequencies yields spurious results. Once the minimum-energy configuration has been calculated, the second step is the determination of interatomic force constants for displacements of the atomic nuclei from their equilibrium positions. Finally, the vibrational frequencies or densities of states are determined from force constants and appropriate isotopic masses (Baroni et al., 2001). Uncertainties in calculated frequencies are typically the main factor limiting the accuracy of calculated fractionation factors. Méheut et al. (2009) showed that a systematic correction of n% on the frequencies induces a relative systematic correction on the logarithmic β-factors ($\ln\beta$) between n% (at low temperatures) to 2n% (at high temperatures). The commonly used generalized gradient approximation is for instance associated with a systematic underestimation of ~5% of the harmonic vibrational frequencies. This would lead to a relative uncertainty of ~0.25‰ on a β-factor of 5‰. A virtue of the theoretical approach is that it enables to go beyond the average isotopic properties of one phase by providing the contribution of each crystallographic site. These data allow to identify the crystal chemical factors governing the isotope fractionations.

14.3.2. NRIXS Spectroscopy

Iron-57 being a Mössbauer-active isotope with a low-lying nuclear excited state at 14.4125 keV, one can use the synchrotron radiation technique of nuclear resonant inelastic X-ray scattering (NRIXS) to probe the vibrational properties of iron contained in a solid. The energy of the incoming X-ray photon beam is changed in small steps within a typical interval of –120 to +150 meV (the exact energy range depends on the temperature of the measurements and the nature of the material analyzed) around the nominal resonance energy (i.e., 14.4125 keV). At each energy, the scattered X-rays induced by the nuclear transition are analyzed. When the pulse hits the sample, X-rays are scattered by electrons. This electronic contribution, almost instantaneous, can be discarded by imposing some time discrimination, while the targeted nuclear scattering is delayed due to the finite lifetime (141 ns) of the excited ^{57}Fe nucleus.

When the incoming X-ray's energy is lower than the nominal resonance energy, some nuclear transitions can still occur because lattice vibrations provide the small energy deficit (a phenomenon known as phonon annihilation). When the incoming energy is higher than the nominal resonance energy, the excess energy can be absorbed by lattice vibrations (phonon creation) and the nuclear transitions can still take place. By measuring the flux of the scattered X-rays for various values of the incident X-ray energy, one can thus probe the vibrational properties of the sample, which in turn are used to determine equilibrium fractionation factors. In practice, two approaches exist to retrieve β-factors from NRIXS spectra. Polyakov et al. (2007) used the kinetic energy and first order perturbation theory to calculate the β-factor from the vibrational density of state of the iron sublattice $g(e)$ (Equations 14.5 and 14.6). The vibrational density of states is calculated using a Fourier-Log transformation of the raw spectrum $S(e)$. Dauphas et al. (2012) used a different approach based on the determination of the force constant of iron bonds and other higher order moments of the raw spectrum $S(e)$. The two approaches are mathematically equivalent (Dauphas et al., 2012). A virtue of the second approach is that the error bars are easy to calculate and one knows how data processing affects the results. The following uncertainties are propagated and details on the error propagation calculation are provided in Dauphas et al. (2014) and Hu (2016): counting statistics, uncertainties in the baseline definition, offset in energy scaling, overall energy scaling, and a bin-to-bin energy jitter. In order to retrieve reliable β-factors, special attention must be paid to the energy range that must be extended enough (as mentioned) and to the baseline definition (Blanchard et al., 2015). The reason is that the mean force constant of the iron bonds, which is the main driver for the isotopic fractionation, is calculated from the third moment of the raw spectrum $S(e)$ or the second moment of the phonon density of states [integrals of S(e) e^3 and $g(e)\,e^2$] such that small errors at the energy tails of the spectra, where is signal is lowest, have a disproportionate influence on the calculated force constant (Dauphas et al., 2012; Blanchard et al., 2015).

14.4. IRON ISOTOPE STUDIES BASED ON NRIXS OR DFT

Two main factors can influence the force constant of the iron bonding environment in condensed phases or fluids: (i) the oxidation state of the metal center; and (ii) the coordination environment, including number and identity of the coordinating ligands. Several DFT studies focused on the magnitude of ligand effect relative to redox effect on Fe isotope fractionation by considering various Fe species relevant of aqueous solutions, such as aquo complexes (Anbar et al., 2005; Ottonello & Zuccolini, 2009)

as well as inorganic and organic complexes (Domagal-Goldman & Kubicki, 2008; Hill & Schauble, 2008; Ottonello & Zuccolini, 2008; Hill et al., 2010; Fujii et al., 2014). Other DFT studies focused on iron-bearing minerals such as hematite, goethite, pyrite, and siderite (Blanchard et al., 2009, 2010, 2015). In particular, Blanchard et al. (2010) tackled the question of the effect of the chemical composition by evaluating the Fe β-factor of hematite (Fe_2O_3) as a function of the Al content. Rustad and collaborators (Rustad & Dixon, 2009; Rustad et al., 2010) studied specifically the mineral-solution isotopic fractionation between aqueous iron and hematite, siderite, or goethite (mainly combining their well-tested β-factors for aqueous iron with previous mineral β-factors). In this case, determining accurate values requires special care because of the fundamentally different nature of the iron-bearing species considered, i.e., a periodic crystal versus a disordered solvated species. Rustad and Yin (2009) investigated the isotopic properties of ferropericlase and ferroperovskite (bridgmanite) in lower-mantle conditions to discuss Earth's accretion and differentiation.

Ab initio studies can most directly be compared with NRIXS studies. Indeed, this synchrotron radiation technique can measure the phonon density of states, which can be compared with theoretical estimates to assess what vibration modes control the isotopic fractionation. Polyakov et al. (2007) and Polyakov and Soultanov (2011) estimated the Fe β-factors of oxide and sulfide minerals from the vibrational densities of states collected in earlier studies whose aims were to derive seismic velocities. Dauphas et al. (2012) also used previously published data in order to document the equilibrium fractionation factors of various compounds among which mainly silicate, oxide, sulfide minerals, and the different phases of metallic iron. They also introduced a new approach to derive equilibrium fractionation factors for iron that involves using the moments of phonon excitation probability density function (as well as the phonon density of states) to calculate the coefficients in the $1/T^2$ polynomial expansion of 1000 lnβ. Dauphas et al. (2012) reported the first NRIXS measurements of goethite and jarosite, which were subsequently reevaluated in Blanchard et al. (2015). This study highlighted the need to collect data over a wide energy range and implemented new data reduction approaches to retrieve accurate β-factors from the NRIXS measurements. Significant improvements have been made to the acquisition and reduction of NRIXS data that have been implemented in a data reduction software called SciPhon (Dauphas et al., 2018).

Roskosz et al. (2015) analyzed by NRIXS a series of spinels with varying compositions and redox states. These Fe β-factors combined with NRIXS data on olivine (Dauphas et al., 2014) and pyroxenes (Jackson et al., 2009) allowed the authors to shed new light on the isotopic signatures of natural peridotites. Several studies addressed the question of metal-silicate fractionation in order to improve our understanding of the conditions of Earth's core formation. Polyakov (2009) calculated the Fe β-factors for metallic iron, ferropericlase, perovskite, and post-perovskite in high-pressure conditions. Some of these NRIXS spectra were acquired for the determination of seismic velocities, which are derived by fitting the PDOS by a Debye model at low energy. The signal-to-noise ratio at those low energies is high and little attention was paid in those studies to the high energy end of the spectra where the signal-to-noise is low. The experiments are done in Diamond Anvil Cells (DACs) with small sample sizes, resulting in long acquisition times. To cut acquisition times, many spectra were truncated in energy before the counts reached background level. As mentioned earlier, this can lead to erroneous estimates of Fe β-factors. More recently, Shahar et al. (2016) investigated the pressure effect (from 2 to 40 GPa) on the iron isotopic properties of iron alloys with hydrogen, carbon, or oxygen. Liu et al. (2017) focused on the fractionation between basaltic glasses, metallic iron and ion-rich alloys of Fe-Ni-Si, Fe-Si, and Fe-S up to 206 GPa. Yang et al. (2018) studied Fe isotopic fractionation in lower mantle minerals bridgmanite and ferropericlase to evaluate whether terrestrial magma ocean crystallization could have imparted some iron isotopic fractionation to Earth's upper mantle. Finally, Dauphas et al. (2014) was interested in the fractional crystallization of magmas and the trend toward heavy iron isotopic compositions of silicic magmas. To do so, these authors determined the Fe β-factors in basaltic, andesitic, dacitic and rhyolitic glasses (taken as proxies for silicate melts) at magmatic temperatures, as well as in olivine. Williams et al. (2016) studied of the iron isotopic properties of silicate glasses but this time with compositions relevant to lunar petrology, which includes mare basalts that are richer in titanium than their terrestrial equivalents.

14.5. COMPARISON OF EQUILIBRIUM FRACTIONATION FACTORS DERIVED FROM VARIOUS TECHNIQUES

Table 14.1 displays a comparison of the iron β-factors obtained from NRIXS, Mössbauer measurements, and first-principles calculations (DFT) for various iron-bearing minerals, i.e., sulfides, oxides, and one carbonate. With the exception of goethite, the β-factors derived from the various techniques are in good agreement. With a maximum difference of 0.5‰ at 298 K, the values are the same within the error bars. In the case of pyrite, the apparent discrepancy between DFT and Mössbauer results that were reported in Blanchard et al. (2009) and

Table 14.1 Iron β-factors ($^{56/54}$Fe) derived from first-principles calculations (DFT), NRIXS, and Mössbauer measurements for some minerals. Error bars due to uncertainties on calculated frequencies or on the data processing for NRIXS and Mössbauer measurements are of the order of ±0.2–0.4‰ at 298 K and ±0.01–0.02‰ at 1573 K.

	DFT		NRIXS		Mössbauer	
Mineral	298 K	1573 K	298 K	1573 K	298 K	1573 K
Pyrite, FeS_2	9.0[a]	0.33[a]	–	–	9.3[b]	0.35[b]
Chalcopyrite, $CuFeS_2$	5.5[c]	0.20[c]	5.4[c]	0.20[c]	–	–
Siderite, $FeCO_3$	4.1[a]	0.15[a]	–	–	4.1[d]	0.15[d]
Hematite, Fe_2O_3	7.1[a]	0.27[a]	7.4[e]	0.28[e]	7.6[f]	0.28[f]
Goethite, FeOOH	7.3[g]	0.28[g]	8.1[g]	0.31[g]	5.7[d]	0.21[d]
Ferropericlase, $(Mg_{0.75}Fe_{0.25})O$	4.7[h]	–	5.2[i]	–	–	–

[a] Blanchard et al. (2009).
[b] Blanchard et al. (2012).
[c] Polyakov and Soultanov (2011).
[d] Polyakov and Mineev (2000).
[e] Dauphas et al. (2012).
[f] Polyakov et al. (2001).
[g] Blanchard et al. (2015).
[h] Rustad and Yin (2009).
[i] Polyakov (2009).

in Polyakov and Soultanov (2011) could be resolved by using a better constrained temperature dependence of the Mössbauer spectra (Blanchard et al., 2012). Unlike other minerals, a significant discrepancy remains for goethite, where the DFT result is loosely bracketed by Mössbauer and NRIXS data. Calculations would suggest a possible overestimation of the NRIXS value possibly related to the baseline definition between the lattice modes and OH bending modes, which might be enough to obtain this 0.8‰ difference. The intrinsic features of the samples studied by NRIXS and Mössbauer spectroscopy may also contribute to the discrepancy (Blanchard et al., 2015). The comparison of results from these independent techniques provides a means of assessing the reliability of equilibrium isotope fractionation factors. A virtue of NRIXS and *ab initio* studies is that they provide β-factors for individual minerals as opposed to α-factors between minerals that equilibration experiments can measure. The former are more widely applicable than the later as the equilibrium fractionation between any two pair of minerals can be calculated provided that their β-factors are known, while equilibration experiments are only relevant to the mineral pair that has been equilibrated. Nevertheless, equilibration experiments and measurements of minerals in natural samples that are thought to have achieved equilibrium provide some ground-truthing of *ab initio* or NRIXS determinations and these more empirical approaches can tackle problems that are presently not easily handled by the vibrational approaches, notably with regard to isotopic fractionation involving liquids.

Inter-mineral equilibrium iron isotopic fractionation factors have been thoroughly discussed in the literature. We report here only a few examples of comparison between theoretical fractionation factors and experimental data. Many experiments are designed to allow measurement of the isotopic fractionation between iron aqueous species and a coexisting mineral. DFT β-factors of Fe aqueous species are quite variable in the literature, depending on the computational methods and parameters used. For instance, values for $Fe(III)_{aq}$ range from 8.3 to 10.1‰ at 295 K (Anbar et al., 2005; Hill & Schauble, 2008; Ottonello & Zuccolini, 2009; Rustad & Dixon, 2009; Rustad et al., 2010; Fujji et al., 2014). Details about the complications related to the modeling of aqueous species can be found in Blanchard et al. (2017). Among these studies, Rustad et al. (2010) performed a meticulous investigation of the effect of the solvation and basis set size on the isotopic properties of aqueous species. By doing so, these authors could reconcile some of the theoretical and experimental fractionation results. The experimental value of Wiesli et al. (2004) for $Fe(II)_{aq}$-siderite (+0.48±0.22‰ at 293 K) is in excellent agreement with the DFT value (+0.54‰) that one obtains by combining the β-factors of Rustad et al. (2010) and Blanchard et al. (2009) for $Fe(II)_{aq}$ and siderite, respectively. DFT also predicts that pyrite should be enriched in Fe heavy isotopes relative to $Fe(II)_{aq}$ (+1.1‰ at 623 K), which is confirmed by the experimental value of Syverson et al. (2013), i.e. +0.99±0.29‰. For hematite, the agreement is less remarkable. The experimental fractionation of −0.10 ±0.20‰ at 370 K between $Fe(III)_{aq}$ and hematite (Skulan et al., 2002) is consistent within the error bars with the fractionation of +0.22‰ found by considering the NRIXS value of hematite β-factor (Dauphas et al.,

2012), while the DFT value (Blanchard et al., 2009) is slightly larger, i.e. +0.43‰ at 370 K. For goethite, there is a disagreement between DFT, NRIXS, and equilibration experiments (Dauphas et al., 2017), as DFT and NRIXS are off by 2‰ from experimental measurements. The reason for the discrepancy is unclear but we note that the experimentally measured equilibrium isotopic fractionation between $Fe(II)_{aq}$ and ferrihydrite is in line with model predictions for goethite. More comparisons, for low- and high-temperature systems, are reviewed in Dauphas et al. (2017).

14.6. PARAMETERS CONTROLLING EQUILIBRIUM FRACTIONATION FACTORS

Provided that the harmonic approximation is valid, theory predicts that isotopic fractionation should scale with the stiffness of the bonds. The stiffness of the interatomic bonds is quantified by the interatomic force constants F. The β-factors increase proportionally with interatomic force constant (Figure 14.3). In other words, understanding fractionation means understanding the parameters that control the force constants of the bonds involving the element of interest, here iron. Among the available data, the iron sulfide troilite displays the lowest Fe force constant while the highest force constant is found in the ferric end-member of a rhyolitic glass. Some studies (e.g., Young et al., 2015; Macris et al., 2015; Sossi & O'Neill, 2017) employed an ionic model for estimating interatomic force constants and from those, equilibrium fractionation factors. This approach has the advantage of helping identify the crystal chemical parameters governing isotopic fractionation. These analytical expressions of F show that the bond strength is mainly controlled by the charge of the two atoms involved in the bonding and the distance between them.

Figure 14.4a shows the temperature dependence of Fe β-factors of minerals where iron is bonded to oxygen atoms. These minerals belong to various mineral families: oxides, carbonates, silicates, and sulfates. In this figure, the three colors allow to separate the minerals with respect to the oxidation state of iron, i.e., presence of only Fe^{2+}, only Fe^{3+}, or a mixed oxidation state with both Fe^{2+} and Fe^{3+}. Minerals with divalent or trivalent iron form two domains that do not overlap. Minerals where iron is divalent display the smallest β-factors, bracketed by siderite at the bottom and olivine, enstatite at the top. Minerals with trivalent iron show larger β-factors, ranging from hematite to jarosite. In this context, the β-factors of minerals with mixed oxidation states (magnetite and spinels) fall in the lower part of the Fe^{3+} domain. Consistently, Macris et al. (2015) measured inter-mineral iron isotopic fractionation from five distinct mantle xenolith lithologies from San Carlos (Arizona) and found that, in all cases where spinel and olivine coexist, the isotopic composition of spinel is heavier than that of the corresponding olivine. The overall picture is that iron oxidation state plays a great role, even if, as we will see, the interatomic force constant is governed by an interplay of several parameters defining the coordination environment (charge, coordination number, bond lengths).

Expectedly, the correlation "β-factor versus force constant" (Figure 14.3) holds for all minerals and melts where iron is bonded to oxygen as well as sulfur. However, the iron sulfides do not follow the trend "β-factor versus

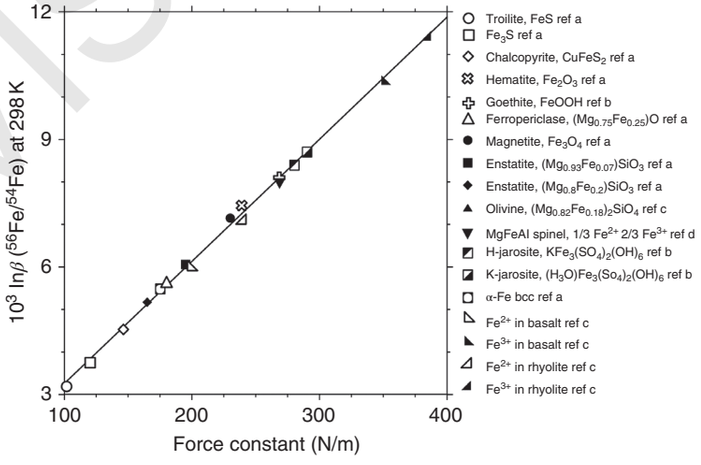

Figure 14.3 Iron β-factors ($^{56/54}$Fe) at 298 K as a function of the iron force constant in various minerals and melts. Data are from the following NRIXS studies: a = Dauphas et al. (2012); b = Blanchard et al. (2015); c = Dauphas et al. (2014); d= Roskosz et al. (2015). Error bars are of the order of ±10 N/m and ±0.2–0.4‰ at that temperature.

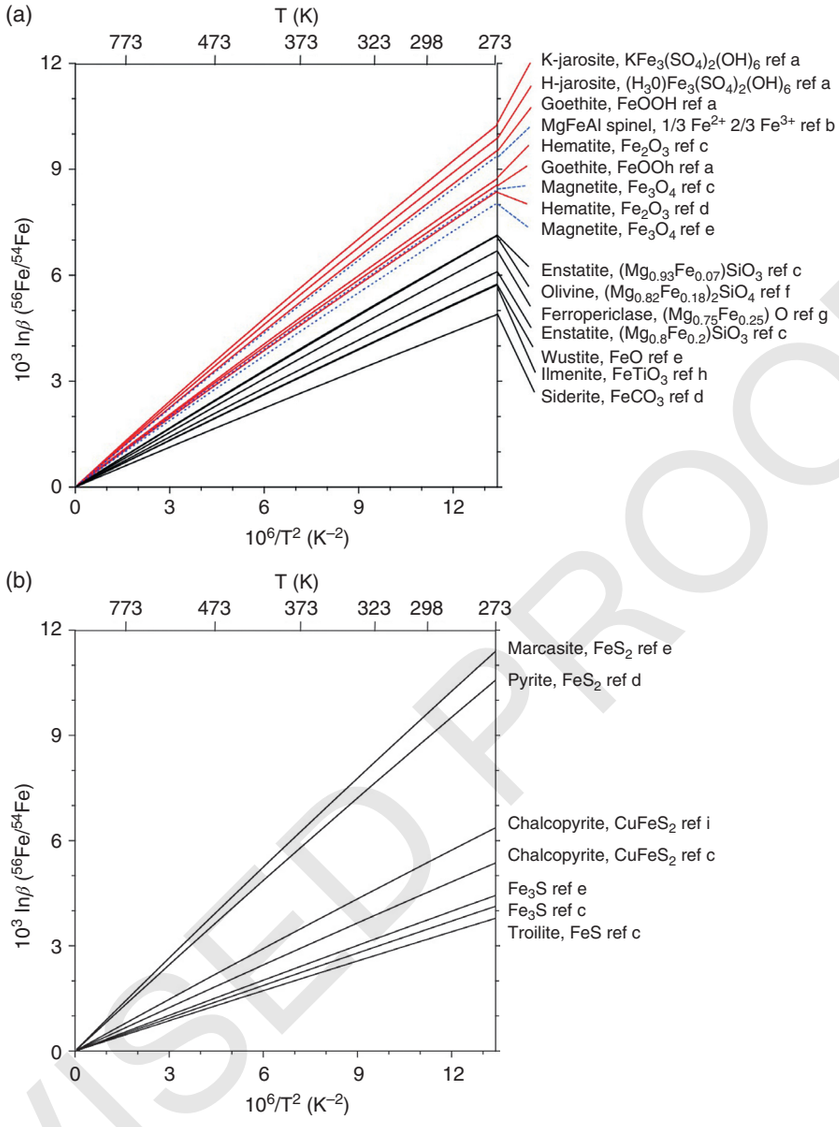

Figure 14.4 Temperature dependence of iron β-factors ($^{56/54}$Fe) for minerals where iron is bonded to oxygen atoms (a) or to sulfur atoms (b). Black curves are for minerals with only Fe^{2+}, red curves for minerals with only Fe^{3+}, and dotted blue curves for minerals with both Fe^{2+} and Fe^{3+}. Data are derived from either first-principles calculations or NRIXS measurements, and are taken from the following references: a = Blanchard et al. (2015); b= Roskosz et al. (2015); c = Dauphas et al. (2012); d = Blanchard et al. (2009); e = Polyakov et al. (2007); f = Dauphas et al. (2014); g = Polyakov (2009); h = Williams et al. (2016); i = Polyakov and Soultanov (2011).

redox state of iron" highlighted for minerals with Fe-O bonds (Figure 14.4) and are also out of the trend "β-factor versus bond length" shown in Figure 14.5. For instance, the two polymorphs pyrite and marcasite with divalent iron ions display β-factors higher than those of all Fe^{3+}-rich oxides and sulfates. This is explained by differing chemical properties of Fe-S bond with respect to Fe-O bond. Fe-S bonds are more covalent than Fe-O bonds as shown by the smaller electronegativy difference (Pauling electronegativities: Fe = 1.83, O = 3.44, S = 2.58). This example shows that at a given redox state, the value of Fe β-factors increase with the degree of covalence of interatomic bonds. We also observe in Figure 14.4 that β-factors of iron sulfides vary over a range of values exceeding that of minerals with Fe-O bonds. Troilite possesses iron as Fe^{2+} in octahedral site like pyrite and

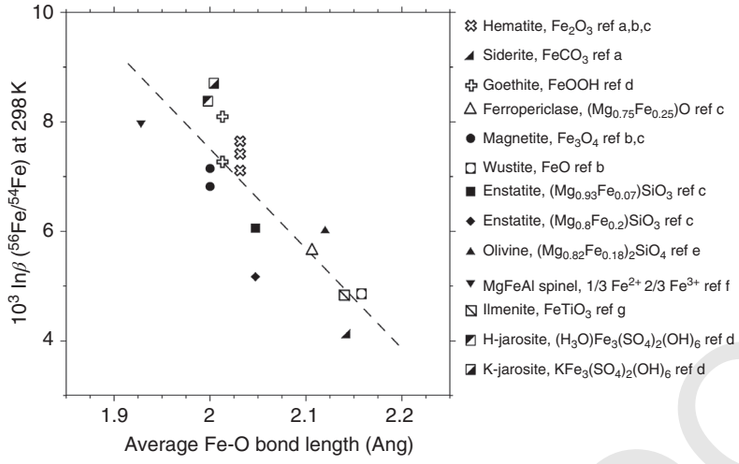

Figure 14.5 Iron β-factors ($^{56/54}$Fe) at 298 K as a function of the average Fe-O bond length for various minerals. Data are derived from either first-principles calculations or NRIXS measurements, and are taken from the following references: a = Blanchard et al. (2009); b = Polyakov et al. (2007); c = Dauphas et al. (2012); d = Blanchard et al. (2015); e = Dauphas et al. (2014); f= Roskosz et al. (2015); g = Williams et al. (2016). The dashed line is a guide for the eye showing the negative correlation trend.

marcasite but in troilite, FeS_6 octahedra are much more distorted and with longer Fe-S bonds, which explains the very low Fe β-factor of troilite. In chalcopyrite, iron is in tetrahedral site but with Fe-S bonds of similar lengths as in marcasite. Chalcopyrite mainly differs by its complex charge distribution between Fe, Cu, and S atoms, where iron would be in high-spin Fe^{3+} state compared to low-spin Fe^{2+} of pyrite and marcasite (Kobayashi et al., 2004). Finally, Fe_3S is the most iron-rich iron sulfide known to date in the iron-sulfur system (Lin et al., 2004). Iron sits in three nonequivalent crystallographic sites with both S and Fe atoms in the first coordination sphere.

Figure 14.5 gives the dependence of Fe β-factors over the average Fe-O bond lengths in minerals. We observe a general decrease of fractionation factors when the average bond length increases, which is in agreement with the general rule of short bonds concentrating heavy isotopes. Bond lengths increase with the coordination number. In this series of minerals, only magnetite and spinels have iron in tetrahedral sites in addition to octahedral sites. The presence of these tetrahedral sites leads to a shortening of the average Fe-O bond length to values lower than 2 Å. Bond lengths are also affected by iron oxidation state. In Figure 14.5, data with an average Fe-O bond length longer than 2.04 Å correspond to minerals containing only divalent iron. Ionic radii are negatively correlated with charge. This plot has been drawn from the crystallographic data usually derived from X-ray diffraction. When Fe presents a partial occupancy of its crystallographic site, like for instance in olivine where Fe shares the metal site with Mg, X-ray diffraction data give an average bond length for this site and without distinguishing Fe from Mg. Therefore, the Fe-O bond lengths are not known accurately. This uncertainty adds to the intrinsic scatter of this relationship. Note that in Figure 14.5, the two enstatite samples differing by their iron content have distinct β-factors. The sample with 7 mol% of Fe displays at 298 K a Fe β-factor 0.9‰ larger than the sample with 20 mol% of Fe. This difference exceeds the error bars of these NRIXS data (Dauphas et al., 2012). Although additional data are required, this effect of the composition may be real. The actual Fe-O bond lengths and thus the force constant and equilibrium isotope fractionation may vary with the Fe content. Similarly, Wang et al. (2017) found using DFT that equilibrium Ca isotope fractionation between pyroxenes depends on the Ca content.

The conclusions regarding the parameters controlling isotopic fractionation, discussed here mainly from mineral data, also hold for magmas. By combining NRIXS and X-ray absorption spectroscopy (XANES) on a series of magmatic glasses, Dauphas et al. (2014) could demonstrate the controls exerted by redox and structural (e.g., polymerization) conditions in magmas. In particular, a structural change of Fe^{2+} in the most silicic magma explains the shift towards higher force constant for Fe^{2+} of the trend defined by rhyolite glasses relative to the single trend defined for basalt, andesite, and dacite glasses.

14.7. SELECTED APPLICATIONS TO THE INTERPRETATION OF IRON ISOTOPIC VARIATIONS IN IGNEOUS ROCKS

Equilibrium fractionation factors have found many applications in low-temperature geochemistry, but kinetic effects are often confounding factors in trying to interpret iron isotopic variations in aqueous systems, products of alteration, or chemical sediments. In that respect, igneous rocks are potentially simpler to interpret. The reason is that in those settings, equilibrium isotopic fractionation between coexisting phases is more easily achieved because diffusion between phases is rapid at high temperature. Kinetic effects are also present but these are mostly due to diffusion, which can be identified by correlating the isotopic variations of one element with another. For example, during diffusion in olivine, Mg and Fe diffuse in opposite directions, resulting in a negative correlation between Mg and Fe isotopic variations (Teng et al., 2011). *In situ* isotopic analyses can also reveal whether kinetic effects are present as the presence of isotopic variations within minerals indicates that the rock is not in isotopic equilibrium (Sio et al., 2013; Oeser et al., 2015). For all these reasons, igneous isotopic geochemistry is a field where determination of iron β-factors is of broad relevance. This is a rapidly expanding field (see Young et al., 2015; Sossi et al., 2016; Dauphas et al., 2017; Bourdon et al., 2018, for some recent reviews on the topic) and we focus on three geological settings where iron isotope geochemistry and redox behavior may play some roles.

14.7.1. Mineral-Melt Fractionation and the Heavy Fe Isotopic Composition of the Crust

The isotopic reference material used for reporting Fe isotopic analyses is IRMM-014. Measurements of chondritic (undifferentiated) meteorites showed that they have similar Fe isotopic composition in bulk and that this composition is indistinguishable from the IRMM-014 value (Craddock & Dauphas, 2011). Mid-ocean ridge basalts have approximately uniform Fe isotopic composition (average $\delta^{56}Fe = +0.105\pm0.006‰$; Teng et al., 2013), which is markedly heavier than chondrites. MORBs are the most abundant constituent of the oceanic crust, meaning that the bulk oceanic crust as a whole must have a heavy Fe isotopic composition. Continental crust also has heavy Fe isotopic composition (Telus et al., 2012).

The question of the Fe isotopic composition of the mantle is more difficult to tackle. Two categories of samples are best suited for that purpose. One is products of high degree partial melting such as komatiites (Dauphas et al., 2010; Hibbert et al., 2012). The reason is that any melt-solid fractionation would be mitigated if a large fraction of the rock melts (in the limit that the mantle is fully molten, then the magma composition must be equal to that of the source rock). A potential issue with komatiites is that they have been weathered and serpentinized but Craddock et al. (2013) showed that serpentinization had little effect on the Fe isotopic composition of abyssal peridotites. Even well-preserved komatiite samples show Fe isotopic variations resulting from partial melting and fractional crystallization (Hibbert et al., 2012), which complicates estimation of the mantle $\delta^{56}Fe$ value. With these caveats in mind, Dauphas et al. (2010) used Alexo komatiites to estimate that the Fe isotopic composition of the mantle must be $+0.044\pm0.030‰$. Magnesium isotopes show little variations in the komatiites measured so far, defining a mantle $\delta^{26}Mg$ value of $-0.275\pm0.042‰$, which is in line with measurements of peridotites (Handler et al., 2009; Teng et al., 2010). Another category of samples is mantle peridotites (Weyer & Ionov, 2007; Poitrasson et al., 2013; Craddock et al., 2013). The problem with these samples is that many samples have been affected by various forms of metasomatism, which fractionates iron isotopes, possibly due to kinetic effects such as diffusive processes in reactions involving melts and minerals (Weyer & Ionov, 2007; Poitrasson et al., 2013). Nevertheless, the distribution of $\delta^{56}Fe$ values of peridotites seems to peak at the chondritic value (Craddock et al., 2013; Poitrasson et al., 2013). In particular, abyssal peridotites, which may sample the mantle source of MORBs have Fe isotopic compositions that are close to chondritic (Craddock et al., 2013). Those data suggest that Earth's mantle has a chondritic Fe isotopic composition of $+0.025\pm0.025‰$ (however, see Poitrasson et al., 2013, for a different viewpoint). Why then does the oceanic crust have heavy Fe isotopic composition?

Three studies have been performed recently to measure the force constant of iron at high pressure by NRIXS (Shahar et al., 2016; Liu et al., 2017, Yang et al., 2018). These studies focused on iron alloys and they found that given the high equilibration temperature involved, partitioning between mantle and core (with O, Si, or Ni as the most likely alloying elements), or terrestrial magma ocean crystallization did not fractionate iron isotopes by more than ~0.02‰. This is consistent with the view that Earth's mantle has a chondritic or slightly elevated $\delta^{56}Fe$ value.

Available evidence suggests that melting the mantle to make the oceanic crust can fractionate iron isotopes. The effect is subtle (~0.07‰) but given that iron is a major constituent of the Earth, understanding what causes this fractionation may shed some light on the processes governing Earth's magmatic evolution. Two approaches have been used to address this question. One is to use estimated equilibrium fractionation between minerals and melts based on measured isotopic variations in peridotites (Williams et al., 2005). This is a proper first-order approach but

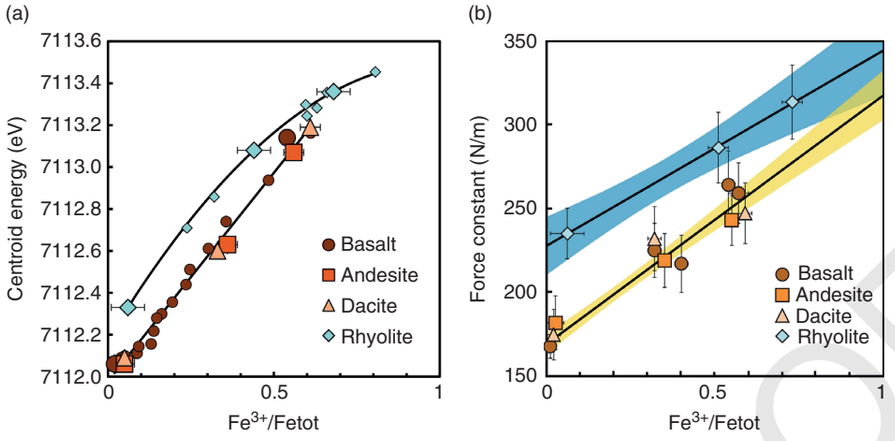

Figure 14.6 XANES centroid energy (left) and mean force constant of iron measured by NRIXS (right) against iron redox state in a variety of synthetic glasses (from Dauphas et al., 2014). The Fe^{3+}/Fe^{2+} ratio has a very strong influence on the stiffness of the iron bonds but superposed on this effect is a control of the silica or alkali content of the melt, as illustrated by the fact that the rhyolite evolves on a different trend than less silicic magma (Source: Dauphas et al., 2014. Reproduced with permission of Elsevier).

to gain a more mechanistic understanding of iron isotopic fractionation during mantle melting, one needs to independently determine the equilibrium fractionation factors between the phases involved.

The main mineral phases relevant to mantle melting to form MORBs are olivine, orthopyroxene, clinopyroxene spinel, and of course basaltic melt. MORBs form by approximately 10% partial melting. Iron in the upper mantle is mostly present as Fe^{2+} (only ~3.5% of iron is in its most oxidized form, Fe^{3+}). The effective melt/solid partition coefficient of iron during melting is ~1, meaning that when 10% of the mantle melts, 10% of iron is partitioned into the melt. This means that to explain the +0.07‰ difference in Fe isotopic composition between mantle and MORBs, a fractionation of approximately +0.07‰ between melt and residue is needed. To our knowledge, no *ab initio* calculations have been performed for iron-bearing minerals relevant to the upper-mantle. There is a more extensive data set available from NRIXS studies (Dauphas et al., 2014; Roskosz et al., 2015; Jackson et al., 2009). Jackson et al. (2009) examined the force constant of iron in orthoenstatite (an orthopyroxene). No data is available for clinopyroxene. Roskosz et al. (2015) studied Fe-bearing spinels characterized by a range of iron contents and oxidation states. Dauphas et al. (2014) measured the force constants of olivine as well as several glasses of basalt, andesite, dacite, and rhyolite containing variable amounts of Fe^{3+}. Prissel et al. (2018) measured the force constant of iron bonds in Fe^{2+}-bearing basaltic glasses doped with various amounts of Ti. The precision of these NRIXS measurements is limited to ~±15 N/m, which translates into an error on the β-factor of ~±0.017‰ at 1300 °C. As discussed in Section 14.6, what emerges from those studies and other experimental studies is that there is a very strong influence of the redox state of iron and a subtler effect of the coordination environment (Figure 14.6). Most phases relevant to mantle are silicates (pyroxenes, olivine, and melt). All Fe^{2+}-bearing phases (minerals and glasses) have Fe force constants that are similar, meaning that taken at face value, little isotopic fractionation is expected between Fe^{2+} in olivine or pyroxene, and Fe^{2+} in melt but higher precision measurements would be needed to tell exactly if any effect is present at the ~±0.03‰ level. Prissel et al. (2018) recently determined experimentally the equilibrium Fe isotopic fraction between silicate melts and olivine and found no measurable fractionation between the two.

A significant effect can be driven by redox conditions as Fe^{3+} tends to be enriched in the heavy Fe isotopes relative to Fe^{2+} and during melting Fe^{3+} behaves as a mildly incompatible element, meaning that the melt will have a higher Fe^{3+}/Fe^{2+} than the solid residue. Dauphas et al. (2009, 2014) assessed the degree of iron isotopic associated with this phenomenon. The result of this analysis is that the NRIXS measurements can only explain approximately half of the isotopic fractionation between melt and mantle (assuming that the mantle has near chondritic Fe isotopic composition). It is not clear at the present time what the cause for the discrepancy is. It could be that clinopyroxenes are enriched in the heavy isotopes of iron, that the harmonic approximation breaks down near or above the solidus, or that kinetic isotope effects are present. Clearly, more work is needed.

14.7.2. Isotopic Fractionation During Magmatic Differentiation

Several studies have shown that rocks related by trends of magmatic differentiation can have fractionated iron isotopic compositions (Teng et al., 2008; Schuessler et al., 2009). In some instances, those trends are not due to equilibrium isotopic fractionation but rather to kinetic isotopic fractionation associated with diffusion in olivine (Dauphas et al., 2010; Teng et al., 2011; Sio et al., 2013, 2018; Sio & Dauphas, 2017; Oeser et al., 2015, 2018; Collinet et al., 2017). As olivine crystallizes, the Mg/Fe of the magma decreases (olivine is relatively Mg-rich). The core of the olivine crystals are therefore out of thermodynamic equilibrium and Fe diffuses in while Mg diffuses out of olivine to correct the existing chemical imbalance between olivine rim and core. Because light Mg and Fe isotopes tend to diffuse faster than heavy isotopes, and Mg and Fe diffuse in opposite directions (Richter et al., 2009), olivine acquires light Fe and heavy Mg isotopic compositions. Removal of such olivine drives the residual magma towards heavy Fe isotopic composition. Diffusive fractionation will only play a role when the timescale for intra-mineral diffusive equilibration is commensurate with the timescale of cooling/crystallization. If the diffusive timescale is much shorter than the cooling/crystallization timescale, then bulk crystals will be in bulk chemical and isotopic equilibrium with the host lava. If the diffusive timescale is much longer than the cooling/crystallization timescale, then the crystal rim will be in equilibrium with the host lava and the crystal interior will be unaffected by diffusive re-equilibration. In the latter case, the bulk of the crystals will not be in equilibrium with the host lava but the relevant isotopic fractionation factors will still be the equilibrium ones, the difference being that the process will be modelled as a distillation.

Equilibrium isotopic fractionation factors are relevant to intra-crustal differentiation of mafic and felsic rocks. One aspect that has a dramatic effect on iron isotopic fractionation is that iron tends to form stronger bonds in more silicic and alkali-rich magmas such as rhyolite than in less silicic and alkali-rich magmas such as basalt (Dauphas et al., 2014). Changes in the coordination environment of iron in these silicic magmas is also seen in XANES (Figure 14.6). During fractional crystallization, the melt-mineral equilibrium isotopic fractionation for iron will thus increase as the crystallization proceeds. This process can produce silica-rich melts that have very heavy Fe isotopic compositions (Dauphas et al., 2014), which are found in natural systems (Poitrasson & Freydier, 2005; Telus et al., 2012). Redox conditions could also influence indirectly how iron isotopes are fractionated during differentiation of mafic and felsic rocks. The reason is that the redox state and whether or not the system is buffered influences the Fe^{3+}/Fe^{2+} ratio in the melt and the onset of magnetite crystallization (Sossi et al., 2012; Foden et al., 2015) and sulfide saturation (Williams et al., 2018; Peters et al., 2018).

14.7.3. Isotopic Fractionation in Arc Lavas

The systematics of iron isotope variations in subduction-related rocks has been the focus of significant work (Dauphas et al., 2009; Foden et al., 2018; Nebel et al., 2013, 2015; Williams et al., 2004, 2005, 2018; Debret et al., 2016). One reason is that these variations are presumably related to the mantle redox conditions and prior history of melting in the source of arc lavas. Oceanic arc lavas are produced by melting of the mantle wedge bounded above by the crust above and below by the subducting slab. This process of flux melting involves the transfer of fluids from the cold subducting plate into the hotter mantle wedge above, where melting takes place primarily due to lowering of the solidus temperature by fluid addition. Arc lavas are more oxidized than MORBs and an outstanding question is whether this is a feature of the source or whether it is an artifact from shallow level degassing and crystallization (Kelley & Cottrell, 2009; Lee et al., 2005).

Williams et al. (2004, 2005) first showed that redox conditions could influence iron isotopic fractionation in arc systems. They measured the Fe isotopic of bulk rocks and mineral separates of sub-arc peridotites and found that the Fe isotopic composition was correlated with the redox state. Specifically, spinels with higher Fe^{3+}/Fe_{tot} ratios had more negative $\delta^{56}Fe$ values than the samples with lower Fe^{3+}/Fe_{tot}. This result is counter intuitive because as discussed in Section 14.6, ferric iron tends to concentrate heavy iron isotopes in spinels and melts (Dauphas et al., 2014; Roskosz et al., 2015). A possible explanation for the trend seen by Williams et al. (2004) is that the peridotites record a prior episode of melt extraction under higher oxygen fugacity. Because Fe^{3+} is incompatible, the Fe^{3+}/Fe^{2+} ratio is higher in the melt than in the solid. Elevated oxygen fugacity is associated with a greater difference in Fe^{3+}/Fe^{2+} between melt and solid, and a larger net equilibrium isotopic fractionation between melt and solid. Melt extraction under high oxygen fugacity can lead to a negative shift in the $\delta^{56}Fe$ value of the residue because the melt is enriched in the heavy isotopes of iron. Negative $\delta^{56}Fe$ values could thus be associated with high Fe^{3+}/Fe_{tot} ratios.

Significant work has also been done on arc lavas (Dauphas et al., 2009; Foden et al., 2018; Nebel et al., 2015; Williams et al., 2018). As discussed, measurements of island arc lavas show that they are more oxidized than MORBs. To first order, one would therefore expect those arc lavas to be enriched in the heavy isotopes of iron,

which is opposite to what is found. Arc lavas tend to have lower δ^{56}Fe values than MORBs. In the New-Britain island arc, the lavas formed by the largest amount of fluid fluxing and highest degree of partial melting are the ones that have δ^{56}Fe values closer to chondritic, while the ones with the lowest degree of partial melting have δ^{56}Fe values closer to MORB (Dauphas et al., 2009). The δ^{56}Fe measurements of island arc basalts from Dauphas et al. (2009) could be interpreted in two ways. One is that island arc basalts actually form under rather low oxygen fugacity so that the isotopic fractionation during melting is small and their oxygen fugacity increases by shallow processes such as degassing and fractional crystallization. The other is that the source of island arc basalts experienced previous episodes of melting, which drove the residue towards lower δ^{56}Fe values (Nebel et al., 2015; Foden et al., 2018). Those low δ^{56}Fe mantle regions could be re-melted to produce island arc basalts. An observation that speaks against the second scenario is that boninites, which are thought to form by high degree flux melting of depleted sources, have remarkably uniform Fe isotopic composition (Dauphas et al., 2009). Furthermore, their δ^{56}Fe value is close to that inferred for the mantle from peridotite measurements (Dauphas et al., 2009). It would take a remarkable coincidence for boninites to originate from a low δ^{56}Fe mantle region and to have then their Fe isotopic compositions shifted by partial melting by just the right amount to end up with such homogeneous and chondritic-like Fe isotopic composition. This is a circumstantial argument, and the second scenario is still viable (Nebel et al., 2015; Foden et al., 2018). Foden et al. (2018) measured the Fe isotopic compositions of mafic lavas from 15 arcs. Like Dauphas et al. (2009), they found that contrary to expectations given their oxidized nature, arc lavas have light Fe isotopic composition relative to MORBs. They also found that across various arcs, the Fe isotopic composition tends to correlate inversely with indirect proxies for the slab transport of oxidants. Cold and wetter subduction systems tend to have the lightest Fe isotopic composition and vice versa. This is more consistent with a scenario that involves large extents of prior melt depletion under buffered oxygen fugacity conditions. Williams et al. (2018) studied extensively the Fe isotopic composition of lavas from the Marianas, focusing in particular on the effect of magmatic differentiation on iron isotopic fractionation in arc settings. In more evolved samples (MgO<~4 wt%), they found significant Fe isotopic fractionation that could be explained by sequestration of magnetite crystals and sulfidic melts. To summarize, redox conditions in the mantle wedge seem to influence the isotopic composition of arc-related lavas but the relationship may be more complex than equating oxidizing conditions in the source to heavier Fe isotopic composition in the lava.

14.8. CONCLUSIONS AND PERSPECTIVES

Iron has received a great deal of attention due to its abundance and importance in all terrestrial reservoirs. Among non-traditional stable isotopes, iron is the most extensively studied element. First-principles calculations and NRIXS measurements are contributing significantly to that field, and fully complement laboratory exchange experiments. Inter-comparisons between all available techniques demonstrate that calculated equilibrium isotopic fractionation factors are reliable enough for interpreting iron isotope variations measured on natural samples. First-principles calculations and NRIXS measurements on well-characterized samples represent efficient tools to understand how crystal chemical parameters control iron isotopic fractionations. Alternatively, an ionic model based on Pauling's rules can be used to get a first-order estimate of the iron β-factor. This approach is satisfactory (at least qualitatively) when the interatomic bonds of interest are ionic but must be taken with care in other cases.

The central parameter controlling the equilibrium fractionation is the interatomic force constant, which reflects the strength of the bonds involving iron. For compounds (minerals, glasses) with relatively ionic Fe-O bonds, the iron oxidation state as well as the Fe-O bond length (in relation with the iron coordination number) will strongly affect the force constant. Whereas the higher degree of covalency of Fe-S bonds explains the singularity of iron sulfides with respect to the trend defined for other compounds involving Fe-O bonds.

Given the richness and complexity of iron chemistry, an extensive set of highly precise and accurate equilibrium fractionation factors is needed to properly interpret natural iron isotopic variations. Special efforts should be made to investigate the effect on isotopic fractionation of the chemical composition (e.g., solid-solutions, chemical impurities) and pressure. To our knowledge, no first-principles calculations have been done to calculate the β-factor of iron in silicate melts. This would be an important direction of investigation even if the quite complex relevant chemistry and redox state of silicate melts, and their high viscosity compared to aqueous solutions represent tremendous challenges for molecular dynamics simulations.

Studies of igneous rocks show that the redox state of iron influences the isotopic composition of iron. This is most clearly seen in arc-related lavas, where recycling of oxidants at subduction zones imparts a specific Fe isotopic signature to the erupted lavas. However, the relationship between redox state in the source and iron isotopic composition of the lavas is complex, reflecting long-term redox conditions in the mantle wedge during prior episodes of melt extraction. The bulk of Earth's oceanic crust has heavy Fe isotopic composition relative

to the inferred mantle composition. While significant progress has been made on that front, the underlying mechanism for this enrichment is still uncertain. Silicic rocks can show heavy Fe isotope enrichments reflecting the fact that iron tends to form stiffer bonds in more silicic and alkali rich magmas. In those systems, redox conditions can also influence the pattern of iron isotopic fractionation by controlling the timing of magnetite crystallization. To summarize, there are many lines of evidence showing that iron isotopes are influenced by redox conditions in igneous rock and significant progress has already been made towards understanding these controls through *ab initio* and NRIXS studies of equilibrium fractionation factors.

ACKNOWLEDGEMENTS

This work was supported by grants from NSF (EAR1444951, EAR1502591) and NASA (NNX17AE86G, NNX17AE87G, NNX15AJ25G, 80NSSC17K0744, 80NSSC20K0821) to ND. We are grateful to Paolo Sossi and an anonymous reviewer for their constructive comments.

REFERENCES

Anbar, A. D., Jarzecki, A. A., & Spiro, T. G. (2005). Theoretical investigation of iron isotope fractionation between $Fe(H_2O)_6^{3+}$ and $Fe(H_2O)_6^{2+}$: implications for iron stable isotope geochemistry. *Geochimica et Cosmochimica Acta*, *69*, 825–837. https://doi.org/10.1016/j.gca.2004.06.012

Baroni, S., de Gironcoli, S., Dal Corso, A., & Giannozzi, P. (2001). Phonons and related crystal properties from density functional perturbation theory. *Reviews of Modern Physics*, *73*, 515–561.

Bigeleisen, J., & Mayer, M. G. (1947). Calculation of equilibrium constants for isotopic exchange reactions. *Journal of Chemical Physics*, *15*, 261–267. https://doi.org/10.1063/1.1746492

Blanchard, M., Poitrasson, F., Méheut, M., Lazzeri, M., Mauri, F., & Balan, E. (2009). Iron isotope fractionation between pyrite (FeS_2), hematite (Fe_2O_3) and siderite ($FeCO_3$): A first-principles density functional theory study. *Geochimica et Cosmochimica Acta*, *73*, 6565–6578. https://doi.org/10.1016/j.gca.2009.07.034

Blanchard, M., Morin, G., Lazzeri, M., & Balan, E. (2010). First-principles study of the structural and isotopic properties of Al- and OH-bearing hematite. *Geochimica et Cosmochimica Acta*, *74*, 3948–3962. https://doi.org/10.1016/j.gca.2010.04.018

Blanchard, M., Poitrasson, F., Méheut, M., Lazzeri, M., Mauri, F., & Balan, E. (2012). Comment on "New data on equilibrium iron isotope fractionation among sulfides: Constraints on mechanisms of sulfide formation in hydrothermal and igneous systems" by V. B. Polyakov and D. M. Soultanov. *Geochimica et Cosmochimica Acta*, *86*, 182–195. doi: 10.1016/j.gca.2012.01.048

Blanchard, M., Dauphas, N., Hu, M., Roskosz, M., Alp, E., Golden, D., et al. (2015). Reduced partition function ratios of iron and oxygen in goethite. *Geochimica et Cosmochimica Acta*, *151*, 19−33. https://doi.org/10.1016/j.gca.2014.12.006

Blanchard, M., Balan, E., & Schauble, E. A. (2017). Equilibrium fractionation of non-traditional isotopes: A molecular modeling perspective. *Reviews in Mineralogy and Geochemistry "Non-traditional stable isotopes," 82*, 27–63. https://doi.org/10.2138/rmg.2017.82.2

Bourdon, B., Roskosz, M., & Hin, R. C. (2018). Isotope tracers of core formation. *Earth-Science Reviews*, *181*, 61–81. https://doi.org/10.1016/j.earscirev.2018.04.006

Collinet, M., Charlier, B., Namur, O., Oeser, M., Médard, E., & Weyer, S. (2017). Crystallization history of enriched shergottites from Fe and Mg isotope fractionation in olivine megacrysts. *Geochimica et Cosmochimica Acta*, *207*, 277–297. https://doi.org/10.1016/j.gca.2017.03.029

Craddock, P. R., & Dauphas, N. (2011). Iron isotopic compositions of geological reference materials and chondrites. *Geostandards and Geoanalytical Research*, *35*, 101−123. https://doi.org/10.1111/j.1751-908X.2010.00085.x

Craddock, P. R., Warren, J. M., & Dauphas, N. (2013). Abyssal peridotites reveal the near-chondritic Fe isotopic composition of the Earth. *Earth and Planetary Science Letters*, *365*, 63−76. https://doi.org/10.1016/j.epsl.2013.01.011

Cygan, R. T., & Kubicki, J. D. (2001). Molecular modeling theory: Applications in the geosciences. *Reviews in Mineralogy and Geochemistry*, *42*, 531.

Dauphas, N., & Rouxel, O. (2006). Mass spectrometry and natural variations of iron isotopes. *Mass Spectrometry Reviews*, *25*, 515–550. https://doi.org/10.1002/mas.20078

Dauphas, N., Craddock, P. R., Asimow, P. D., Bennett, V. C., Nutman, A. P., & Ohnenstetter, D. (2009). Iron isotopes may reveal the redox conditions of mantle melting from Archean to Present. *Earth and Planetary Science Letters*, *288*, 255−267. https://doi.org/10.1016/j.epsl.2009.09.029

Dauphas, N., Teng, F.-Z., & Arndt, N. T. (2010). Magnesium and iron isotopes in 2.7 Ga Alexo komatiites: Mantle signatures, no evidence for Soret diffusion, identification of diffusive transport in zoned olivine. *Geochimica et Cosmochimica Acta*, *74*, 3274−3291. https://doi.org/10.1016/j.gca.2010.02.031

Dauphas, N., Roskosz, M., Alp, E., Golden, D., Sio, C., Tissot, F., et al. (2012). A general moment NRIXS approach to the determination of equilibrium Fe isotopic fractionation factors: application to goethite and jarosite. *Geochimica et Cosmochimica Acta*, *94*, 254−275. https://doi.org/10.1016/j.gca.2012.06.013

Dauphas, N., Roskosz, M., Alp, E. E., Neuville, D., Hu, M., Sio, C. K., et al. (2014). Magma redox and structural controls on iron isotope variations in Earth's mantle and crust. *Earth and Planetary Science Letters*, *398*, 127–140. https://doi.org/10.1016/j.epsl.2014.04.033

Dauphas, N., John, S. G., & Rouxel, O. (2017). Iron isotope systematics. *Reviews in Mineralogy and Geochemistry "Non-traditional stable isotopes," 82*, 415–510. https://doi.org/10.2138/rmg.2017.82.11

Dauphas, N., Hu, M. Y., Baker, E. M., Hu, J., Tissot, F. L. H., Alp, E. E., et al. (2018). SciPhon: a Data Analysis Software for Nuclear Resonant Inelastic X-ray Scattering with Applications to Fe, Kr, Sn, Eu and Dy. *Journal of Synchrotron*

Radiation, *25*, 5, 1581–1599. https://doi.org/10.1107/S1600577518009487

Debret, B., Millet, M.-A., Pons, M.-L., Bouihol, P., Inglis, E., & Williams, H. (2016). Isotopic evidence for iron mobility during subduction. *Geology*, *44*, 215−218. https://doi.org/10.1130/G37565.1

Domagal-Goldman, S. D., & Kubicki, J. D. (2008). Density functional theory predictions of equilibrium isotope fractionation of iron due to redox changes and organic complexation. *Geochimica et Cosmochimica Acta*, *72*, 5201–5216. https://doi.org/10.1016/j.gca.2008.05.066

Foden, J., Sossi, P. A., & Wawryk, C. M. (2015). Fe isotopes and the contrasting petrogenesis of A-, I-and S-type granite. *Lithos*, *212*, 32−44. https://doi.org/10.1016/j.lithos.2014.10.015

Foden, J., Sossi, P. A., & Nebel, O. (2018). Controls on the iron isotopic composition of global arc magmas. *Earth and Planetary Science Letters*, *494*, 190–201. https://doi.org/10.1016/j.epsl.2018.04.039

Fujii, T., Moynier, F., Blichert-Toft, J., & Albarède, F. (2014). Density functional theory estimation of isotope fractionation of Fe, Ni, Cu, and Zn among species relevant to geochemical and biological environments. *Geochimica et Cosmochimica Acta*, *140*, 553–576. https://doi.org/10.1016/j.gca.2014.05.051

Handler, M. R., Baker, J. A., Schiller, M., Bennett, V. C., & Yaxley, G. M. (2009). Magnesium stable isotope composition of Earth's upper mantle. *Earth and Planetary Science Letters*, *282*, 306–313. https://doi.org/10.1016/j.epsl.2009.03.031

Hibbert, K., Williams, H., Kerr, A. C., & Puchtel, I. (2012). Iron isotopes in ancient and modern komatiites: evidence in support of an oxidised mantle from Archean to present. *Earth and Planetary Science Letters*, *321*, 198−207. https://doi.org/10.1016/j.epsl.2012.01.011

Hill, P. S., & Schauble, E. A. (2008). Modeling the effects of bond environment on equilibrium iron isotope fractionation in ferric aquo-chloro complexes. *Geochimica et Cosmochimica Acta*, *72*, 1939–1958. doi: 10.1016/j.gca.2007.12.023

Hill, P. S., Schauble, E. A., & Young, E. D. (2010). Effects of changing solution chemistry on Fe^{3+}/Fe^{2+} isotope fractionation in aqueous Fe–Cl solutions. *Geochimica et Cosmochimica Acta*, *74*, 6669–6689. https://doi.org/10.1016/j.gca.2010.08.038

Hohenberg, P., & Kohn, W. (1964). Inhomogeneous electron gas. *Physical Review*, *136*, B864−B871. https://doi.org/10.1103/PhysRev.136.B864

Hu, M. Y. (2016). Some notes on data analysis for nuclear resonant inelastic x-ray scattering. *Hyperfine Interact*, *237*, 64. https://doi.org/10.1007/s10751-016-1284-7

Jackson, J. M., Hamecher, E. A., & Sturhahn, W. (2009). Nuclear resonant X-ray spectroscopy of $(Mg,Fe)SiO_3$ orthoenstatites. *European Journal of Mineralogy*, *21*, 551–560. https://doi.org/10.1127/0935-1221/2009/0021-1932

Johnson, C. M., Beard, B. L., Roden, E. E. (2008). The iron isotope fingerprints of redox and biogeochemical cycling in modern and ancient Earth. *Annual Review of Earth and Planetary Sciences*, *36*, 457–493. https://doi.org/10.1146/annurev.earth.36.031207.124139

Kelley, K. A., & Cottrell, E. (2009). Water and the oxidation state of subduction zone magmas. *Science*, *325*, 605–607. doi: 10.1126/science.1174156

Kieffer, S. W. (1982). Thermodynamics and lattice vibrations of minerals: 5. Applications to phase equilibria, isotopic fractionation, and high-pressure thermodynamic properties. *Reviews of Geophysics and Space Physics*, *20*, 827–849. https://doi.org/10.1029/RG020i004p00827

Kobayashi, H., Kamimura, T., Alfé, D., Sturhahn, W., Zhao, J., & Alp, E. E. (2004). Phonon density of states and compression behavior in iron sulfide under pressure. *Physical Review Letters*, *93*, 195503. doi: 10.1103/PhysRevLett.93.195503

Lee, C.T., Leeman, W. P., Canil, D., & Li, Z.-X. A. (2005). Similar V/Sc systematics in MORB and arc basalts: Implications for the oxygen fugacities of their mantle source regions. *Journal of Petrology*, *46*, 2313–2336. https://doi.org/10.1093/petrology/egi056

Lin, J.-F., Fei, Y., Sturhahn, W., Zhao, J., Mao, H., & Hemley, R. J. (2004). Magnetic transition and sound velocities of Fe3S at high pressure: implications for Earth and planetary cores. *Earth and Planetary Science Letters*, *226*, 33–40. https://doi.org/10.1016/j.epsl.2004.07.018

Lipkin, H. J. (1995). Mössbauer sum rules for use with synchrotron sources. *Physical Review B*, *52*, 10073. doi: 10.1103/physrevb.52.10073

Lipkin, H. J. (1999). Mössbauer sum rules for use with synchrotron sources. *Hyperfine Interactions*, *123–124*, 349–366. https://doi.org/10.1023/A:1017019822825

Liu, J., Dauphas, N., Roskosz, M., Hu, M. Y., Yang, H., Bi W., et al. (2017). Iron isotopic fractionation between silicate mantle and metallic core at high pressure. *Nature Communications*, *8*, 14377. https://doi.org/10.1038/ncomms14377

Macris, C. A., Manning, C. E., & Young, E. D. (2015). Crystal chemical constraints on inter-mineral Fe isotope fractionation and implications for Fe isotope disequilibrium in San Carlos mantle xenoliths. *Geochimica et Cosmochimica Acta*, *154*, 168–185. https://doi.org/10.1016/j.gca.2015.01.024

Méheut, M., Lazzeri, M., Balan, E., & Mauri, F. (2009). Structural control over equilibrium silicon and oxygen isotopic fractionation: a first-principles density-functional theory study. *Chemical Geology*, *258*, 28–37. https://doi.org/10.1016/j.chemgeo.2008.06.051

Moynier, F., Fujii, T., Wang, K., & Foriel, J. (2013). Ab initio calculations of the Fe(II) and Fe(III) isotopic effects in citrates, nicotianamine, and phytosiderophore, and new Fe isotopic measurements in higher plants. *Comptes Rendus Géoscience*, *245*, 230–240. https://doi.org/10.1016/j.crte.2013.05.003

Nebel, O., Arculus, R., Sossi, P., Jenner, F., & Whan, T. (2013). Iron isotopic evidence for convective resurfacing of recycled arc-front mantle beneath back-arc basins. *Geophysical Research Letters*, *40*, 5849−5853. https://doi.org/10.1002/2013GL057976

Nebel, O., Sossi, P., Bénard, A., Wille, M., Vroon, P., & Arculus, R. (2015). Redox-variability and controls in subduction zones from an iron-isotope perspective. *Earth and Planetary Science Letters*, *432*, 142−151. https://doi.org/10.1016/j.epsl.2015.09.036

Oeser, M., Dohmen, R., Horn, I., Schuth, S., & Weyer, S. (2015). Processes and time scales of magmatic evolution as revealed by Fe–Mg chemical and isotopic zoning in natural

olivines. *Geochimica et Cosmochimica Acta*, *154*, 130−150. https://doi.org/10.1016/j.gca.2015.01.025

Oeser, M., Ruprecht, P., & Weyer, S. (2018). Combined Fe-Mg chemical and isotopic zoning in olivine constraining magma mixing-to-eruption timescales for the continental arc volcano Irazú (Costa Rica) and Cr diffusion in olivine. *American Mineralogist*, *103*, 4, 582–599. https://doi.org/10.2138/am-2018-6258

Ottonello, G., & Zuccolini, M. V. (2008). The iron-isotope fractionation dictated by the carboxylic functional: An ab-initio investigation. *Geochimica et Cosmochimica Acta*, *72*, 5920–5934. https://doi.org/10.1016/j.gca.2008.09.027

Ottonello, G., & Zuccolini, M. V. (2009). Ab-initio structure, energy and stable Fe isotope equilibrium fractionation of some geochemically relevant H–O–Fe complexes. *Geochimica et Cosmochimica Acta*, *73*, 6447–6469. https://doi.org/10.1016/j.gca.2009.06.034

Peters, B. J., Shahar, A., Carlson, R. W., Day, J. M. D., & Mock, T. D. (2019). A sulfide perspective on iron isotope fractionation during ocean island basalt petrogenesis. *Geochimica et Cosmochimica Acta*, *245*, 59–78. https://doi.org/10.1016/j.gca.2018.10.015

Poitrasson, F., Halliday, A. N., Lee, D.-C., Levasseur, S., & Teutsch, N. (2004). Iron isotope differences between Earth, Moon, Mars and Vesta as possible records of contrasted accretion mechanisms. *Earth and Planetary Science Letters*, *223*, 253–266. https://doi.org/10.1016/j.epsl.2004.04.032

Poitrasson, F., & Freydier, R. (2005). Heavy iron isotope composition of granites determined by high resolution MC-ICP-MS. *Chemical Geology*, *222*, 132−147. https://doi.org/10.1016/j.chemgeo.2005.07.005

Poitrasson, F., Delpech, G., & Grégoire, M. (2013). On the iron isotope heterogeneity of lithospheric mantle xenoliths: implications for mantle metasomatism, the origin of basalts and the iron isotope composition of the Earth. *Contributions to Mineralogy and Petrology*, *165*, 1243−1258. https://doi.org/10.1007/s00410-013-0856-7

Polyakov, V. B. (1997). Equilibrium fractionation of the iron isotopes: Estimation from Mössbauer spectroscopy data. *Geochimica et Cosmochimica Acta*, *61*, 4213–4217. https://doi.org/10.1016/S0016-7037(97)00204-4

Polyakov, V. B. (2009). Equilibrium iron isotope fractionation at core-mantle boundary conditions. *Science*, *323*, 912–914. doi: 10.1126/science.1166329

Polyakov, V. B., & Mineev, S. D. (2000). The use of Mössbauer spectroscopy in stable isotope geochemistry. *Geochimica et Cosmochimica Acta*, *64*, 849–865. https://doi.org/10.1016/S0016-7037(99)00329-4

Polyakov, V. B., Mineev, S. D., Gurevich, V. M., Khramov, D. A., Gavrichev, K. S., Gorbunov, V. E., & Golushina, L. N. (2001). The use of Mössbauer spectroscopy and calorimetry for determining isotopic equilibrium constants. *Hematite. Russian Journal of Physical Chemistry*, *75*, 912–916.

Polyakov, V. B., Mineev, S. D., Clayton, R. N., Hu, G., & Mineev, K. S. (2005). Determination of tin equilibrium isotope fractionation factors from synchrotron radiation experiments. *Geochimica et Cosmochimica Acta*, *69*, 5531–5536. https://doi.org/10.1016/j.gca.2005.07.010

Polyakov, V., Clayton, R., Horita, J., & Mineev, S. (2007). Equilibrium iron isotope fractionation factors of minerals: reevaluation from the data of nuclear inelastic resonant X-ray scattering and Mössbauer spectroscopy. *Geochimica et Cosmochimica Acta*, *71*, 3833−3846. https://doi.org/10.1016/j.gca.2007.05.019

Polyakov, V. B., & Soultanov, D. M. (2011). New data on equilibrium iron isotope fractionation among sulfides: constraints on mechanisms of sulfide formation in hydrothermal and igneous systems. *Geochimica et Cosmochimica Acta*, *75*, 1957–1974. https://doi.org/10.1016/j.gca.2011.01.019

Prissel, K. B., Krawczynski, M. J., Nie, N. X., Dauphas, N., Couvy, H., Hu, M. Y., et al. (2018). Experimentally determined effects of olivine crystallization and melt titanium content on iron isotopic fractionation in planetary basalts. *Geochimica et Cosmochimica Acta*, *238*, 580–598. https://doi.org/10.1016/j.gca.2018.07.028

Richet, P., Bottinga, Y., & Javoy, M. (1977). A review of hydrogen, carbon, nitrogen, oxygen, sulphur, and chlorine stable isotope fractionation among gaseous molecules. *Annual Reviews of Earth and Planetary Sciences*, *5*, 65–110.

Richter, F. M., Watson, E. B., Mendybaev, R., Dauphas, N., Georg, B., Watkins, J., & Valley, J. (2009). Isotopic fractionation of the major elements of molten basalt by chemical and thermal diffusion. *Geochimica et Cosmochimica Acta*, *73*, 4250−4263. https://doi.org/10.1016/j.gca.2009.04.011

Roskosz, M., Sio, C. K. I., Dauphas, N., Bi, W., Tissot, F. H. L., Hu, M. Y., et al. (2015). Spinel-olivine-pyroxene equilibrium iron isotopic fractionation and applications to natural peridotites. *Geochimica et Cosmochimica Acta*, *169*, 184–199. https://doi.org/10.1016/j.gca.2015.07.035

Rustad, J. R., & Dixon, D. A. (2009). Prediction of iron-isotope fractionation between hematite (α-Fe_2O_3) and ferric and ferrous iron in aqueous solution from density functional theory. *The Journal of Physical Chemistry A*, *113*, 12249–12255. doi: 10.1021/jp9065373

Rustad, J. R., & Yin, Q.-Z. (2009). Iron isotope fractionation in the Earth's lower mantle. *Nature Geoscience*, *2*, 514–518. https://doi.org/10.1038/ngeo546

Rustad, J. R., Casey, W. H., Yin, Q.-Z., Bylaska, E. J., Felmy, A. R., Bogatko, S. A., et al. (2010). Isotopic fractionation of Mg^{2+}, Ca^{2+}, and Fe^{2+} with carbonate minerals. *Geochimica et Cosmochimica Acta*, *74*, 6301–6323. doi: 10.1016/j.gca.2010.08.018

Saunier, G., Pokrovski, G. S., & Poitrasson, F. (2011). First experimental determination of iron isotope fractionation between hematite and aqueous solution at hydrothermal conditions. *Geochimica et Cosmochimica Acta*, *75*, 6629–6654. https://doi.org/10.1016/j.gca.2011.08.028

Schauble, E. A. (2004). Applying stable isotope fractionation theory to new systems. *Reviews in Mineralogy and Geochemistry*, *55*, 65–111. doi: 10.2138/gsrmg.55.1.65

Schuessler, J. A., Schoenberg, R., Behrens, H., & von Blanckenburg, F. (2007). The experimental calibration of the iron isotope fractionation factor between pyrrhotite and peralkaline rhyolitic melt. *Geochimica et Cosmochimica Acta*, *71*, 417–433. https://doi.org/10.1016/j.gca.2006.09.012

Schuessler, J. A., Schoenberg, R., & Sigmarsson, O. (2009). Iron and lithium isotope systematics of the Hekla volcano, Iceland—evidence for Fe isotope fractionation during magma differentiation. *Chemical Geology*, *258*, 78–91. https://doi.org/10.1016/j.chemgeo.2008.06.021

Shahar, A., Young, E. D., & Manning, C. E. (2008). Equilibrium high-temperature Fe isotope fractionation between fayalite and magnetite: an experimental calibration. *Earth and Planetary Science Letters*, *268*, 330–338. https://doi.org/10.1016/j.epsl.2008.01.026

Shahar, A., Schauble, E. A., Caracas, R., Gleason, A. E., Reagan, M. M., Xiao, Y., et al. (2016). Pressure-dependent isotopic composition of iron alloys. *Science*, *352*, 580–582. 10.1126/science.aad9945

Shahar, A., Elardo S. M., & Macris, C. A. (2017). Equilibrium fractionation of non-traditional stable isotopes: an experimental perspective. *Reviews in Mineralogy and Geochemistry "Non-traditional stable isotopes,"* *82*, 65–83. https://doi.org/10.2138/rmg.2017.82.3

Sio, C. K. I., & Dauphas, N. (2017). Thermal histories of magmatic bodies by Monte Carlo inversion of Mg-–Fe isotopic profiles in olivine. *Geology*, *45*, 67–70. https://doi.org/10.1130/G38056.1

Sio, C. K. I., Dauphas, N., Teng, F.-Z., Chaussidon, M., Helz, R. T., & Roskosz, M. (2013). Discerning crystal growth from diffusion profiles in zoned olivine by in situ Mg–Fe isotopic analyses. *Geochimica et Cosmochimica Acta*, *123*, 302−321. https://doi.org/10.1016/j.gca.2013.06.008

Sio, C. K., Roskosz, M., Dauphas, N., Bennett, N. R., Mock, T., & Shahar, A. (2018). The isotope effect for Mg-Fe interdiffusion in olivine and its dependence on crystal orientation, composition and temperature. *Geochimica et Cosmochimica Acta*, *239*, 463–480. https://doi.org/10.1016/j.gca.2018.06.024

Skulan, J. L., Beard, B. L., & Johnson C. M. (2002). Kinetic and equilibrium Fe isotope fractionation between aqueous Fe(III) and hematite. *Geochimica et Cosmochimica Acta*, *66*, 2995–3015. https://doi.org/10.1016/S0016-7037(02)00902-X

Sossi, P. A., Foden, J. D., & Halverson, G. P. (2012). Redox-controlled iron isotope fractionation during magmatic differentiation: an example from the Red Hill intrusion, S Tasmania. *Contributions to Mineralogy and Petrology*, *164*, 757−772. https://doi.org/10.1007/s00410-012-0769-x

Sossi, P. A., & O'Neill, H.St.C. (2015). The effect of bonding environment on iron isotope fractionation between minerals at high temperature. *Geochimica et Cosmochimica Acta*, *196*, 121–143. https://doi.org/10.1016/j.gca.2016.09.017

Sossi, P. A., Nebel, O., & Foden, J. (2016). Iron isotope systematics in planetary reservoirs. *Earth and Planetary Science Letters*, *452*, 295–308. https://doi.org/10.1016/j.epsl.2016.07.032

Syverson, D. D., Borrok, D. M., & Seyfried, Jr. W. E. (2013). Experimental determination of equilibrium Fe isotopic fractionation between pyrite and dissolved Fe under hydrothermal conditions. *Geochimica et Cosmochimica Acta*, *122*, 170–183. https://doi.org/10.1016/j.gca.2013.08.027

Telus, M., Dauphas, N., Moynier, F., Tissot, F. L., Teng, F.-Z., Nabelek, P. I., et al. (2012). Iron, zinc, magnesium and uranium isotopic fractionation during continental crust differentiation: The tale from migmatites, granitoids, pegmatites. *Geochimica et Cosmochimica Acta*, *97*, 247−265. https://doi.org/10.1016/j.gca.2012.08.024

Teng, F.-Z., Dauphas, N., & Helz, R. T. (2008). Iron isotope fractionation during magmatic differentiation in Kilauea Iki Lava Lake. *Science*, *320*, 1620−1622. doi: 10.1126/science.1157166 *Article*

Teng, F.-Z., Li, W.-Y., Ke, S., Marty, B., Dauphas, N., Huang, S., et al. (2010). Magnesium isotopic composition of the Earth and chondrites. *Geochimica et Cosmochimica Acta*, *74*, 14, 4150–4166. https://doi.org/10.1016/j.gca.2010.04.019

Teng, F.-Z., Dauphas, N., Helz, R. T., Gao, S., & Huang, S. (2011). Diffusion-driven magnesium and iron isotope fractionation in Hawaiian olivine. *Earth and Planetary Science Letters*, *308*, 317−324. https://doi.org/10.1016/j.epsl.2011.06.003

Teng, F.-Z., Dauphas, N., Huang, S., & Marty, B. (2013). Iron isotopic systematics of oceanic basalts. *Geochimica et Cosmochimica Acta*, *107*, 12−26. https://doi.org/10.1016/j.gca.2012.12.027

Urey, H. C. (1947). The thermodynamic properties of isotopic substances. *Journal of the Chemical Society* (London) 562–581.

Wang, W., Zhou, C., Qin, T., Kang, J.-T., Huang, S., Wua, Z., & Huang F. (2017). Effect of Ca content on equilibrium Ca isotope fractionation between orthopyroxene and clinopyroxene. *Geochimica et Cosmochimica Acta*, *219*, 44–56. https://doi.org/10.1016/j.gca.2017.09.022

Weyer, S., & Ionov, D. A. (2007). Partial melting and melt percolation in the mantle: The message from Fe isotopes. *Earth and Planetary Science Letters*, *259*, 119−133. https://doi.org/10.1016/j.epsl.2007.04.033

Wiesli, R. A., Beard, B. L., & Johnson, C. M. (2004). Experimental determination of Fe isotope fractionation between aqueous Fe(II), siderite and "green rust" in abiotic systems. *Chemical Geology*, *211*, 343–362. https://doi.org/10.1016/j.chemgeo.2004.07.002

Williams, H. M., McCammon, C. A., Peslier, A. H., Halliday, A. N., Teutsch, N., Levasseur, S., & Burg, J.-P. (2004). Iron isotope fractionation and the oxygen fugacity of the mantle. *Science*, *304*, 1656−1659. doi: 10.1126/science.1095679

Williams, H. M., Peslier, A. H., McCammon, C., Halliday, A. N., Levasseur, S., Teutsch, N., & Burg, J. P. (2005). Systematic iron isotope variations in mantle rocks and minerals: The effects of partial melting and oxygen fugacity. *Earth and Planetary Science Letters*, *235*, 435−452. https://doi.org/10.1016/j.epsl.2005.04.020

Williams, K. B., Krawczynski, M. J., Nie, N. X., Dauphas, N., Couvy, H., Hu, M. Y. and Alp, E. E. (2016) 'The role of differentiation processes in mare basalt iron isotope signatures', *Lunar Planetary Science Conference*, *47*, pp. 2779

Williams, H. M., Prytulak, J., Woodhead, J. D., Kelley, K. A., Brounce, M., & Plank, T. (2018). Interplay of crystal fractionation, sulfide saturation and oxygen fugacity on the iron isotope composition of arc lavas: An example from the Marianas. *Geochimica et Cosmochimica Acta*, *226*, 224–243. https://doi.org/10.1016/j.gca.2018.02.008

Yang, H., Lin, J.-F., Hu, M. Y., Roskosz, M., Bi, W., Zhao, J., et al. (2018). Iron isotopic fractionation in mineral phases from Earth's lower mantle: Did terrestrial magma ocean crystallization fractionate iron isotopes? *Earth and Planetary Science Letters*, *506*, 113–122. https://doi.org/10.1016/j.epsl.2018.10.034

Young, E. D., Manning, C. E., Schauble, E. A., Shahar, A., Macris, C. A., Lazar, C., & Jordan, M. (2015). High-temperature equilibrium isotope fractionation of non-traditional stable isotopes: Experiments, theory, and applications. *Chemical Geology*, *395*, 176–195. https://doi.org/10.1016/j.chemgeo.2014.12.013